

Manufacturing an active X-ray mirror prototype in thin glass

D. Spiga,^{a*} M. Barbera,^{b,c} A. Collura,^c S. Basso,^a R. Candia,^c M. Civitani,^a
M. S. Di Bella,^c G. Di Cicca,^c U. Lo Cicero,^c G. Lullo,^b C. Pellicciari,^a M. Riva,^a
B. Salmaso,^a L. Sciortino^b and S. Varisco^c

Received 27 July 2015

Accepted 13 September 2015

^aINAF, Osservatorio Astronomico di Brera, Via Bianchi 46, Merate, Italy, ^bUniversità degli Studi di Palermo, Via Archirafi 36, Palermo, Italy, and ^cINAF, Osservatorio Astronomico di Palermo, Piazza del Parlamento 1, Palermo, Italy. *Correspondence e-mail: danielle.spiga@brera.inaf.it

Edited by M. Zangrando, Elettra and IOM-CNR, Italy

Keywords: X-ray mirrors; active optics; thin glass mirrors; piezoelectric actuators.

Adjustable mirrors equipped with piezo actuators are commonly used at synchrotron and free-electron laser (FEL) beamlines, in order to optimize their focusing properties and sometimes to shape the intensity distribution of the focal spot with the desired profile. Unlike them, X-ray mirrors for astronomy are much thinner in order to enable nesting and reduce the areal mass, and the application of piezo actuators acting normally to the surface appears much more difficult. There remains the possibility to correct the deformations using thin patches that exert a tangential strain on the rear side of the mirror: some research groups are already at work on this approach. The technique reported here relies on actively integrating thin glass foils with commercial piezoceramic patches, fed by voltages driven by the feedback provided by X-rays, while the tension signals are carried by electrodes on the back of the mirror, obtained by photolithography. Finally, the shape detection and the consequent voltage signal to be provided to the piezoelectric array will be determined by X-ray illumination in an intra-focal setup at the XACT facility. In this work, the manufacturing steps for obtaining a first active mirror prototype are described.

1. Introduction

The angular resolution of X-ray telescopes is an essential figure of merit for describing the capabilities for detecting X-ray sources in the distant Universe. Since X-ray telescopes operate from space, the achievable angular resolution is not affected by the disturbance of the atmospheric turbulence but only by mirror deformations and surface imperfections, while, owing to the small wavelengths of X-rays, aperture diffraction remains a minor problem at the present state-of-art technology.

Unlike focusing mirrors at work in synchrotron beamlines, mirrors for X-ray telescopes need to be thin and lightweight. Mirror modules are subject to stringent mass limits, but at the same time they need large collecting areas to detect extremely low fluxes from distant astronomical sources. Since in grazing incidence the projected surface along the incidence direction is usually very small, thin mirrors with decreasing diameters ('shells') are nested in the aperture left clear by the previous one, all with the same optical axis and focus. Moreover, in order to keep the mechanical stiffness constant, the mirror wall thickness varies in proportion to the mirror shell radius. In this way, large apertures (up to ~ 1 m) can be effectively filled; the price to pay is twofold, however. First, in a densely nested module X-rays impinge onto the mirrors almost side-



mirror wall thickness. Secondly, the mass/geometric area ratio of a mirror module can be proven (Basso *et al.*, 2008) to be expressed as

$$M/A_{\text{geo}} \approx 8\rho fk, \quad (1)$$

with ρ being the mirror bulk density, f its focal length and k its thickness/radius ratio, assumed to be constant throughout the entire module. Typically, X-ray mirrors have focal lengths ranging from meters (e.g. 1.5 m for eROSITA; Fürmetz *et al.*, 2014) to tens of meters (e.g. 12 m for ATHENA; Collon *et al.*, 2014; Proserpio *et al.*, 2014), so large effective areas imply very high masses unless materials with low ρ and k values are selected. For this reason, the widely used nickel electroforming technique is not viable for large X-ray telescopes like ATHENA. Lightweight materials such as glass, silicon or silicon carbide have to be selected. Finally, the mirrors have to be very thin compared with their linear dimensions, which also entails a lower obstruction of the effective area.

There is another important difference between X-ray optics for astronomy and for ground-based applications: in the former case, a large number of mirrors have to be manufactured, tested and assembled. Moreover, X-ray optical modules of the future will be so ample (e.g. 3 m diameter for ATHENA) that single mirror shells will necessarily be produced in smaller segments formed in the correct shape (e.g. parabola + hyperbola in sequence for the Wolter-I geometry; Van Speybroeck & Chase, 1972), stacked, assembled and accurately aligned. Therefore, the number of individual mirror plates to be produced becomes *very* large. Hence, the selected technology has to comply with stringent requirements for surface smoothness and figure error. At the same time, it should enable an expeditious manufacturing process that can be easily implemented by industries.

For the ATHENA telescope, selected by ESA as a second large-class mission for the 2015–2025 Cosmic Vision plan, with a launch foreseen in 2028, the baseline technology relies on silicon pore optics (SPO; Collon *et al.*, 2014). This approach should be able to reach an angular resolution of 5 arcsec half-energy width (HEW) by 2019. At the same time, the technology of hot slumped glass optics (SGO) is being developed as a backup solution. This technique consists of forming thin glass foils at high temperature onto a cylindrical forming mould, to be later stacked and spaced *via* stiffening glass ribs to form an X-ray optical unit (XOU). Despite the brittleness of thin glass foils, an integrated XOU proved to be able to endure a launch to orbit. In fact, the optical modules of the NuSTAR X-ray telescope, launched and still operational, are exactly made of SGOs (Craig *et al.*, 2011). Furthermore, SGOs have been studied under ESA contract in 2009–2013 at INAF/OAB (Osservatorio Astronomico di Brera; Civitani *et al.*, 2013, 2014) and in parallel at MPE (Max Planck Institute for Extraterrestrial Physics; Proserpio *et al.*, 2014; Winter *et al.*, 2014), producing a number of demonstrators with improving optical quality. An example of XOU manufactured at INAF/OAB and made of four Wolter-I plate pairs is shown in Fig. 1. The typical angular resolutions of the X-ray optics replicated by nickel electroforming have been reached with hot slumped

glasses, but improvements below 20 arcsec HEW will require a more accurate slumping figure. In this regard, the research on SGOs at INAF/OAB is still ongoing and recent developments seem to be moving towards the correct direction (Salmaso *et al.*, 2014).

Regardless of the mirror technology that will be adopted, thin mirrors are very prone to deformation, hence degrading the focal spot size that determines the angular resolution. For this reason, some research groups are at work on the possibility to improve the shape of an X-ray mirror after it has been assembled into the optical module, extending the concept of *active optics* in use for decades in optical astronomy. However, in this case there is no atmospheric disturbance to compensate: it is the mirror figure itself that is corrected using piezoelectric actuators fixed on the non-optical side of the glasses. Research on adjustable X-ray optics has already been pursued by a consortium led by Leicester University (Atkins *et al.*, 2009) and is currently under study at the Center for Astrophysics in Boston (Reid *et al.*, 2014; Schwartz *et al.*, 2014).

There are several problems to face in active optics for X-ray telescopes. One is the dense mirror stacking that implies the absence of a stiff reference plane except for the first mirror plate. This makes the situation rather different from the one experienced at synchrotrons or free-electron lasers (FELs), where a single thick mirror can be adjusted by actuators usually pushing in the normal direction. A solution comes from the adoption of piezoelectric actuators exerting a tangential strain rather than a normal pressure. In this way, one can change the local curvature of the mirror in the longitudinal direction, and also compensate the deformation introduced by the piezo itself (e.g. the shrinkage of the glue).

Another problem, as we will see, is the feedback to the actuators once they have been fixed on the rear side of mirror



Figure 1 An optical module, manufactured at INAF/OAB, made of four stacked pairs of slumped glasses (after Civitani *et al.*, 2013). Each pair is a grazing-incidence parabola–hyperbola system operating two reflections in sequence. Ribs are used to properly space the mirrors and to endow them with the required stiffness.

plates and densely stacked. Under those conditions it is not realistic to systematically rely on metrology tools: optical metrology in visible or UV is also made difficult by the impact of aperture diffraction and, moreover, the reflection of UV light in grazing incidence is usually insensitive to undulations in the centimeter range (usually known as *mid-frequencies*). To minimize the aperture diffraction effects and detect mirror defects down to the centimeter lateral scales, X-rays can be used. This also offers the opportunity to directly test the mirror performances with X-rays and, at the same time, to find the optimal combination of voltages to drive the piezo array. The problem has been faced this way by other groups, but with an intrinsic difficulty: the observation of the point spread function (PSF) in focus does not convey direct information about the mirror defects, because their imprints on the intensity pattern are nearly collapsed to a single point. The search for the optimal voltage array has therefore to be achieved *via* algorithms for the PSF width minimization, usually quite complex, and running the risk of a local minimization.

We hereafter present the activities being carried out at INAF/OAB, Università di Palermo, and INAF/OAPA (Osservatorio Astronomico di Palermo), in the context of the AXYOM (Adjustable X-ray optics for astrOnomy) project, aimed at developing the actuation of thin slumped glass X-ray mirrors using piezoelectric components. Some details have already been presented by Spiga *et al.* (2014). The technology for glass slumping, metrology, integration and testing is already fully developed at INAF/OAB (Pareschi *et al.*, 2011; Civitani *et al.*, 2013): our purpose is to endow these mirrors with actuation capabilities using thin piezoelectric elements acting tangentially. The mirror profile detection and the consequent voltage to be supplied to the piezo array is based on a direct feedback provided by the X-ray illumination of already integrated mirrors. Rather than optimizing the PSF in focus, however, we will observe the variation of the intensity pattern in intra-focal position and infer the local mirror curvature (Spiga *et al.*, 2013a) along various longitudinal profiles. This will allow us to recover the mirror profile and deterministically correct its errors: this non-destructive *in situ* characterization is applicable also to the thick mirrors typically used at synchrotrons/FEL beamlines. Indeed, there is another advantage that ground-based X-ray mirrors might take from this work: for example, mirrors operating at very shallow angles need to be very long in order to collect the full beam aperture: a viable alternative can be a stack of a few shorter mirrors that should be very thin in order to minimize beam obstruction. Hence, the solution described in this paper can be adopted, including a piezo array to correct shape errors.

In this paper we show the production steps of an active X-ray mirror prototype made of a thin slumped glass with two piezo actuators (§2), and describe the method we will adopt for testing and actively correcting the mirror shape errors (§3) at the XACT X-ray facility at INAF/OAPA (Barbera *et al.*, 2006; Collura *et al.*, 1994). The conclusions are briefly summarized in §4.

2. Manufacturing an active mirror prototype

2.1. Hot slumping of a thin glass foil

This piezo-actuated mirror is the first prototype that was produced in the AXYOM project. The first step is represented by the hot glass forming in a cylindrical shape at INAF/OAB laboratories. We have used the standard process, consisting of a 200 mm × 200 mm foil of EAGLE XG[®] by Corning onto a cylindrical mould of K20 ceramic with a 1 m curvature radius. The glass/mould materials were selected not only to avoid sticking at high temperature, which peaks at 750°C, but also for minimizing the difference in the coefficient of thermal expansion (CTE) and the consequent shear of the glass-to-mould interface and the formation of small ripples in the profile. In fact, the thermal cycle lasts several hours in order to allow the ripples to relax. With respect to the hot slumping process for the NuSTAR optics, we exert a pressure on the back of the foil to force the glass-to-mould contact and so improve the shape replication (INAF patent). The pressure ranges between 20 g cm⁻² and 50 g cm⁻², and is realised by pumping down in the muffle just below the glass. In order to maintain the differential pressure, indeed, the glass has to divide the muffle into two sealed chambers, and consequently needs to be formed in a larger size than 200 mm × 200 mm. After the thermal cycle, the formed glass foil is trimmed to its correct dimensions.

The resulting mirror is a sector of a cylinder, with the longitudinal profiles along the axis. Because of unavoidable forming errors, the longitudinal profiles will exhibit deformations of the order of a few micrometers on the full length scale, down to less than one-tenth of a micrometer over a lateral scale of a few centimeters. The subsequent integration (§2.4), anyway, corrects the forming errors to an extent that improves as the nearest rib is approached, hence the maximum error is expected to be mid-way between two adjacent ribs. Moreover, the correction capability is variable for the different Fourier components in the profile: in fact, the defect damping is maximum for the lowest harmonics in the profile (mostly responsible for the peak-to-valley value), while spatial wavelengths in the mid-frequency range remain almost unchanged. More details on the slumping process can be found in Salmaso *et al.* (2014).

2.2. Electrode deposition

The subsequent step is the realisation of contacts for the piezoelectric elements. Wires hanging on the back of the foil would obstruct X-rays in a stack, and would also deform the glass by their weight. We have therefore selected the deposition of contacts directly on the back of the mirror by photolithography. The electrodes are 80 nm of titanium, plus 15 nm of gold to avoid the formation of a native oxide that would hamper the electrical contact. The resulting electrodes (see Fig. 2) supply the voltages to the piezo array from a lateral side, where small wires can be glued *via* conductive epoxy. This side will be deformed by the weight of the cables but, owing to the presence of a stiffening rib just nearby, the deformation will only concern 1 cm of azimuthal aperture after integration,

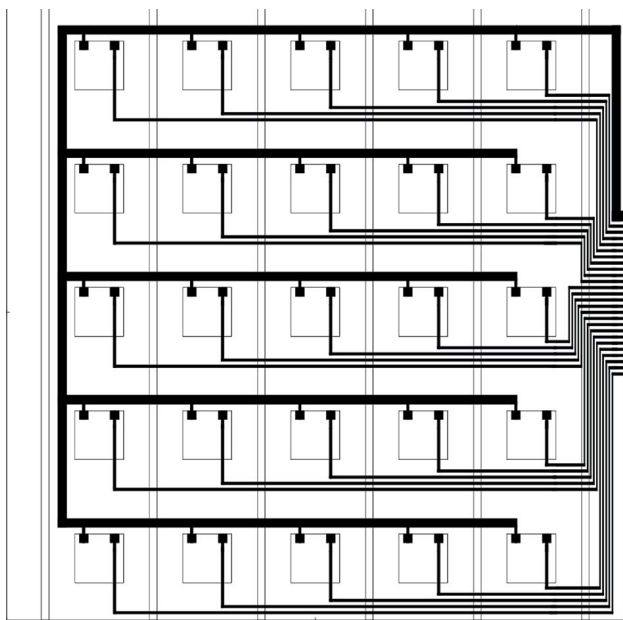


Figure 2
A preliminary pattern of electrodes to be deposited on the back of the glass mirrors. Each square represents a piezoelectric actuator. The vertical sticks represent the ribs.

which can be easily shaded out. The preliminary design foresees a 5×5 matrix of piezoelectric elements, located amid two consecutive ribs, where the profile error is expectedly larger.

Two photolithographic processes have been studied at INAF/OAPA, enabling the electrode printing with the desired pattern on thin glass foils:

(1) *Metal lift-off*. The drawing is printed in negative on transparent paper and the photoresist is sprayed onto the non-optical side of the glass foil. The drawing is then used to mask in contact the photoresist against a UV light, obtaining a 1:1 pattern impression of the circuit pattern, which can be removed with sodium hydroxide at the electrode locations. Two thin layers of titanium and gold are deposited by e-beam evaporation, and finally the photoresist is lifted off by acetone, leaving the metal layers only in correspondence of the tracks.

(2) *Chemical attack*. This alternative process starts from the deposition of evaporated titanium and gold on the rear side of the glass foil, followed by the photoresist spraying. This time, the mask is printed in positive in order to shade from UV light the photoresist where the electrodes have to be deposited. After the UV exposure in the presence of the mask, the photoresist is developed in a solution of sodium hydroxide, leaving the metal exposed where the mask was not present. Etching in aqua regia is used to remove gold in excess, then etching in hydrogen peroxide to remove titanium. Finally, a bath in a solution of sodium hydroxide removes the photoresist residual. This process has returned better results in terms of electrode integrity.

Since the circuit mask is printed in contact with the glass, the aforementioned processes work on both flat or curved foils. There are two possibilities:

(a) Electrode deposition onto a flat $200 \text{ mm} \times 200 \text{ mm}$ glass with subsequent hot slumping in an oven: this method has the



Figure 3
The system of electrodes sketched in Fig. 2, once deposited on the back of a glass foil formed in the shape of a cylindrical sector. The glass is laid upon the mould of K20.

disadvantage of exposing the metallic pattern to very high temperatures, with potential damage or conductivity losses. However, this approach has been followed to produce the mirror shown in Fig. 3, and the tracks were not damaged, excepting a resistance increase to some tens of ohms, that is irrelevant being the resistance of piezos of the order of $10^{10} \Omega$. Another drawback is the impossibility to exert a pressure on the foil during the slumping cycle because the foil is already the final size and cannot be used to seal the lower part of the muffle (§2.1); hence, we can expect a worse optical quality, especially in the mid-frequency content (Ghigo *et al.*, 2013).

(b) Electrode deposition onto an already formed $200 \text{ mm} \times 200 \text{ mm}$ glass foil: this solution enables hot slumping assisted by pressure without the risk of damaging the printed electrodes. There is, however, a higher risk of breaking the glass during the photolithographic process.

The active mirror prototype we describe in this work has been produced using the method 2(b), *i.e.* chemical attack on a formed glass foil. Profile measurement after contact deposition shows that the broader tracks (thick lines in Fig. 2), used as a common electrode, introduce some glass deformation in the longitudinal direction ($0.2 \mu\text{m}$ peak-to-valley over lateral scales of 4 cm) caused by the stress in the metallic layer. Although this adds a 4 arcsec HEW to the shape errors, most of the conductive tracks are thinner and seem not to alter the glass shape. Subsequent tests will be performed reducing the thickness of the common electrodes.

Finally, the glass foil was coated on the optical side by 80 nm of titanium. This is not really needed to enhance the reflectivity in X-rays because, at the X-ray energies we are using (0.3 keV), even a bare glass surface reflects up to incidence angles of 4.5 deg. The Ti layer is necessary, however, in order to suppress the optical light reflection by the back of the glass foil, which would disturb the optical sensors of the profilometers used to assess the piezo effects under variable voltages. This step will be necessary to obtain a preliminary calibration of the influence function of the piezoelectric patches (§2.5).

2.3. Piezoelectric component selection and fixing

Tangentially acting piezoelectric actuators are available commercially. Out of different possibilities (piezopolymers, microfibers, piezoceramics), a finite element modeling (Dell’Agostino *et al.*, 2014) showed that *piezoceramic trans-*


Figure 4

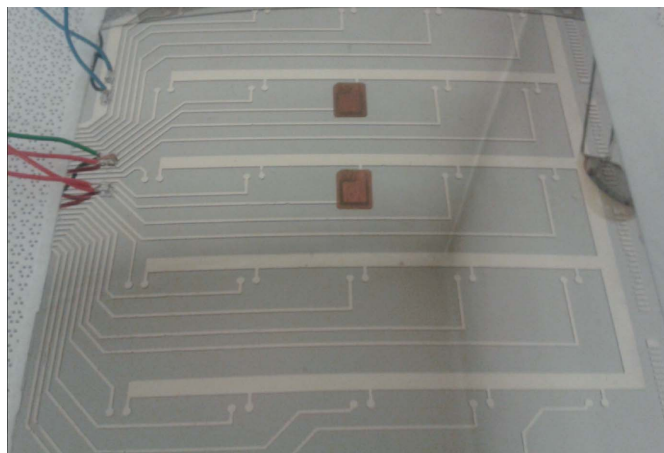
Detail of a P-876.SP1 piezoelectric actuator (size 16 mm × 16 mm) glued onto a couple of electrode contacts, seen through an uncoated glass foil. Electrical contact with the soldering pads of the piezo is ensured *via* two droplets of conductive epoxy glue.

ducers have sufficient bending strengths to correct deformations of a 0.4 mm-thick glass when voltages of a few tens of volts are applied. The piezoceramic element is sold enclosed in Kapton, with two soldering pads for electrical contact on the same side, and can operate in a vacuum. Furthermore, they are flexible enough to be used on curved substrates. We have selected the P-876.SP1 model from Physik Instrumente having a 16 mm × 16 mm size and 200 μm thickness. Their size makes them suitable for profile corrections down to spatial wavelengths of a few centimeters, whilst the low thickness ensures a low shell obstruction in a mirror stack. In reality, this material exerts an isotropic strain in both (longitudinal and sagittal) directions. Fortunately, at the grazing-incidence angle α the correction in the sagittal direction has a lesser weight in the angular resolution, with respect to longitudinal defects, by $\tan 2\alpha$, *i.e.* by almost two orders of magnitude. Finally, in parallel to the P-876.SP1, we are also considering the adoption of the P-876K015 model from the same brand (50 mm × 11 mm). This model will be useful to correct deformations over longer spatial scales, and also to activate a longer fraction of the profile with a smaller number of voltage signals.

For the mirror prototype we are producing we have fixed two P-876.SP1 amid the two central ribs. The glue is a low-shrinkage (0.03%) epoxy resin Masterbond EP30-2, used at INAF/OAB as a standard for the integration of slumped glass foils, deposited in a layer of approximately 75 μm. The electrical contact is obtained by two small drops of conductive epoxy in correspondence with the piezo soldering pads and the electrode terminals (shown in detail in Fig. 4). After the complete polymerization of the glues, the electrical contacts are checked measuring the capacitance at the electrodes connected to the piezos, which should be close to their nominal value (8 nF for the P-876.SP1). Finally, electric wires have been connected to the electrodes using conductive epoxy. The back of the mirror after this step is shown in Fig. 5.

2.4. Mirror integration onto a back plane

After checking the proper operation of the piezoceramic patches, the active mirror was integrated onto an aluminium backplane *via* stiffening ribs. The integration has taken place


Figure 5

The glass foil after forming, printing the electrode pattern, coating the optical side, gluing two piezoelectric patches, and connecting electric wires to the respective electrodes. The blue wire is connected to the grounded electrode.

in the integration machine (IMA; Civitani *et al.*, 2013) at INAF/OAB, in an ISO6 clean room at a controlled temperature of $(20 \pm 0.1)^\circ\text{C}$. The active foil has firstly been forced to adhere to a precisely figured mould in fused silica, in the shape of a paraboloid, *via* vacuum suction. In this way, the shape of the mould is provisionally imparted to the optical side of the foil, including the longitudinal curvature. Ribs in BK7 glass are precisely aligned and glued to the back plane and to the back side of glass (Fig. 6): since the thickness of the glue layer (50–75 μm) is much larger than the sag of the parabolic profile (1 μm) for the mirror radius and the focal length adopted, after the glue curing the shape of the mould is ‘frozen’, at least at the rib locations. When the glass foil is separated from the mould, however, it tends to return to its original shape (including forming errors and the deformation induced by the coating stress) owing to its elastic properties; hence, shape


Figure 6

The active glass foil prototype during integration in the integration machine at INAF/OAB. The ribs are being glued while the optical surface is maintained in contact, *via* vacuum suction, with a precisely figured mould in BK7. The integration process is performed at a $(20 \pm 0.1)^\circ\text{C}$ controlled temperature.

errors are corrected only partially between ribs (§2.1). The scope of this project is the correction of those residual errors, by acting on the piezoelectric actuators.

2.5. Influence function measurement

After the glue polymerization, the operation of the piezos was checked using the long trace profilometer (LTP; Fig. 7). The central glass profile has been measured varying the piezo voltages, observing the profile changes, thereby confirming that the integration did not damage the conductivity of the electrodes. In Fig. 8 we display the optical profile displacement when feeding the piezo B, with respect to the measurement at zero voltage. The voltages are provided by a dedicated electronic board developed for this project, which can manage at the same time up to 16 channels.

As expected, the actuated surface moves upwards for positive voltages with respect to the common electrode. The behavior is nearly symmetric at negative voltages, with very low hysteresis effects and negligible cross-talk. An applied

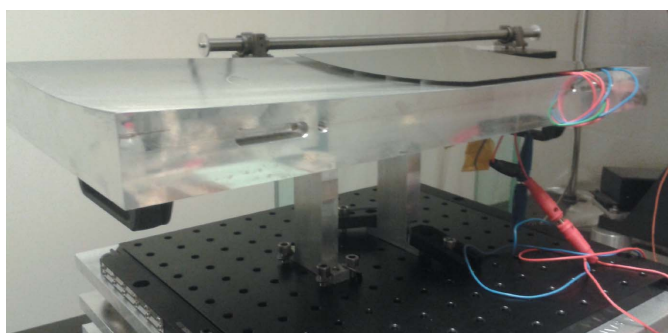


Figure 7
The finally integrated mirror onto the back plane, being aligned under the long trace profilometer at INAF/OAB in order to measure the deformation imparted by piezoelectric patches when fed by a voltage.

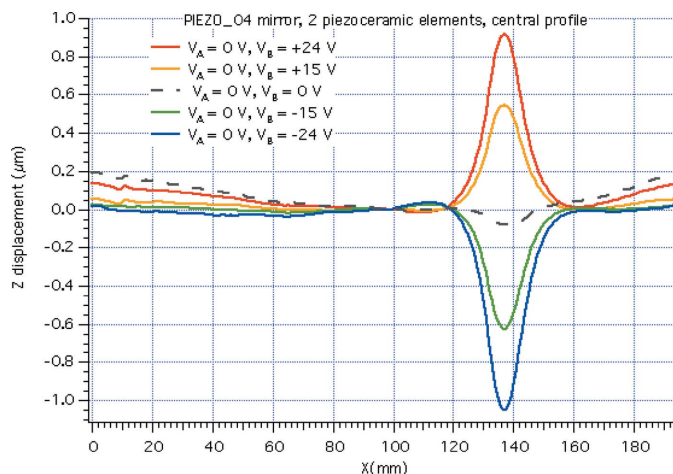


Figure 8
Results of the measurements with the long trace profilometer (Fig. 7), applying a potential difference to the piezo B. The displacements with respect to the initial profile, without voltage applied, are shown. The small dip for $V_B = 0$ is a hysteresis effect. The piezo A is located near $x = 100$ mm and correctly exhibits no displacement if no voltage is applied to it.

voltage of 25 V enables a profile correction of ~ 1 μm , which is much more than the typical error amplitude over the piezo length. We notice, however, that the influence of the piezo is not limited to its surface extent, owing to the relative rigidity of the glass foil: it is apparently extended over a profile length that is at least twice as large. This is a positive aspect since it will expectedly reduce the well known kink effects in the gaps between consecutive piezos. We also notice some limited reaction in the rest of the profile.

3. Test and active profile correction at the XACT facility

Once completed, prototypes of active X-ray mirrors will be tested in X-ray tests in an intra-focus setup using the XACT 35 m-long X-ray facility (Fig. 9) at INAF/OAPA (Barbera *et al.*, 2006; Collura *et al.*, 1994). The facility includes electron impact X-ray sources covering the range 0.1–20 keV, X-ray monochromators, a 35 m high-vacuum (10^{-6} mbar) pipe including three test chambers, vacuum micro-positioning systems and X-ray detectors (including a 4 cm-diameter microchannel plate with a 100 μm pixel size). The test chamber includes a vacuum alt-azimuth mount for precise sample alignment. Our scope is the mirror shape detection under X-ray illumination.

Since the mirror geometry was based on the IXO design (Pareschi *et al.*, 2011) with a focal length $f = 20$ m, the available source-to-detector distance at XACT (35 m) does not enable measurements in focus. In contrast, intra-focal exposures are easy to achieve. Mirror shape reconstruction in X-rays is often obtained in synchrotron light by scanning the surface with a pencil beam and back-tracing the beam from the arrival point on the detector. However, since the beam is quite narrow, the mirror has to be scanned for its surface to be reconstructed; this is possible only if the mirror is precisely positioned and its location/orientation is accurately monitored during the scan. Another method consists of diagnosing the reflected beam with a wavefront sensor, but these devices are in general



Figure 9
The XACT X-ray facility in INAF/OAPA. A 35 m-long vacuum tube is used to illuminate with X-rays the samples in the vacuum chamber, visible in the background.

expensive and the surface profile can be retrieved only using dedicated software.

Under certain conditions, indeed, full-illumination X-ray exposures in an intra-focal setup directly enable the reconstruction of the mirror surface, without making use of the techniques mentioned above: here we just recall the basis of the surface reconstruction formalism, already described in detail elsewhere (Spiga *et al.*, 2013a), postponing the description of the tests at XACT and the results to a subsequent paper. The surface reconstruction is based on the X-ray intensity modulations of the focused beam, observed in an intra-focal position at a distance D from mirror to detector. In fact, a perfect mirror with aperture Δz_m would return an arc of width $w_0 = \Delta z_m(f - D)/f$ and uniform brightness (Fig. 10a). In contrast, the arc reflected by a real mirror exhibits a variable width w and intensity, typically striations oriented in the sagittal direction (see Fig. 10b). The intensity profile in the z direction, $I(z_D)$, can be related to the mirror profile in the longitudinal direction, $z_m(x)$. Actually, a similar approach was used in optical astronomy in the 1980s (Roddier, 1988) as a wavefront sensor. Moreover, we adopted an analogous method to solve beam-shaping problems in focus (Spiga *et al.*, 2013b).

If geometric optics can be applied down to spatial wavelengths covered by the pixel size on the detector and X-ray scattering is negligible, the relation between the mirror slope and the coordinate on the detector, z_D , is

$$z_D(x) = z_m(x) + 2z'_m(x)(D - x). \quad (2)$$

We now introduce the modulation function $M(z_D) = 1 - I_0/I(z_D)$, where I_0 is a constant expressed in terms of measurable quantities:

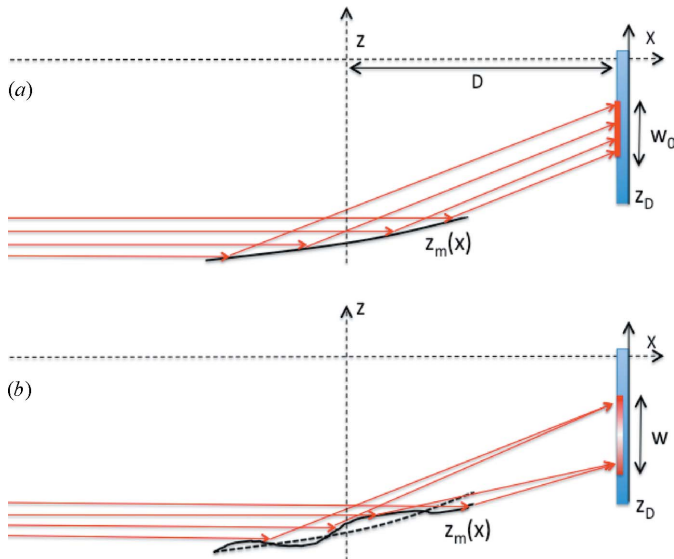


Figure 10
The principle of profile reconstruction in intra-focal setup (after Spiga *et al.*, 2013a). A grazing-incidence mirror is illuminated with X-rays and the reflected beam is collected by an imaging detector in intra-focus position. (a) If the mirror had a perfect shape, the intra-focal image would be uniform. (b) In the presence of mirror deformations, the intensity distribution is modulated as a function of the local curvature in the longitudinal direction.

$$I_0 = \frac{w}{Lz'_m(0)} \left\langle \frac{1}{I(z_D)} \right\rangle^{-1}, \quad (3)$$

$z'_m(0)$ is the mirror slope at $x = 0$, and L the mirror length. The solution of equation (2) is (Spiga *et al.*, 2013a)

$$z'_m(x) = z'_m(0) \exp \left[\int_0^x \frac{M(z_D)}{2(D-t)} dt \right], \quad (4)$$

and the mirror profile is obtained by integration of the slope over x . In equation (4), $z'_m(0)$ is a constant to be determined by constraining the intensity width to return the nominal one,

$$\int_{-L/2}^{+L/2} z'_m(x) dx = L \sin \alpha, \quad (5)$$

and α is the grazing incidence angle on the mirror surface. If $\alpha \approx 2^\circ$ and $D = 5$ m, then spatial wavelengths of 1 cm can be treated geometrically (Raimondi & Spiga, 2015) for X-ray energies higher than 0.1 keV, *e.g.* using the C-K α X-ray line at 0.3 keV.

However, a simple application of equation (4) does not allow us to reconstruct the mirror profile, with the relation between x and $I(z_D)$ being unknown. Fortunately, the correct solution can be approached by successive approximations: first, using the relation for a perfect mirror $z_D = -(w/L)x$, equation (4) returns a zero-order profile $z_{m,0}$. With this function in hand, we compute the expected coordinate set $z_{D,0}(x)$ *via* equation (2), and resample $I(z_D)$ on it. The resampled intensity can now be used to derive an improved profile release $z_{m,1}$ *via* equation (4), from which we can derive a $z_{D,1}(x)$ function, and so on. Typically, the process converges in 10–20 iterations (a satisfactory convergence requires approximately 1 min).

Once the difference between the measured and the desired profile is known, the piezo actuation can be used to perform the correction. As the influence function of the piezos has been preliminarily measured (*e.g.* on representative samples, §2.5), the optimal voltage matrix can be found by a least-squares algorithm.

4. Conclusions

We have described the manufacturing of a first active X-ray mirror prototype for astronomical applications, based on the thin glass slumping technology already developed at INAF/OAB. This mirror includes a preliminary distribution of contacts and only two piezoceramic actuators; nevertheless, their influence could be measured easily by optical profilometry. Even if the thin mirror technology is developed for X-ray telescopes aiming at a low mass/area ratio, applications to synchrotron radiation are also possible, owing to the stacking possibilities offered by the thin mirror technology that enables the coverage of wider apertures than single mirrors, especially at very shallow incidence angles where a large aperture would imply excessive lengths. Moreover, the possibility to drive a piezo array *via* the feedback provided by intra-focal imaging is also applicable to mirrors currently in

use at synchrotron/FEL beamlines. We expect to produce in the next months a more advanced mirror with an improved matrix of piezoelectric patches that will be actively driven in intra-focal setup at the XACT facility.

Acknowledgements

The AXYOM project, devoted to the study of the correction of thin glass/plastic foils for X-ray mirrors, is financed by a TECNO-INAF 2012 grant. M. Zangrando, L. Raimondi, C. Svetina, N. Mahne (ELETTRA Sincrotrone Trieste and IOM-CNR, Italy) and Alexey Vikhlinin (Harvard-Smithsonian Center for Astrophysics) are gratefully acknowledged for encouragement and useful discussions.

References

- Atkins, C., Wang, H., Doel, P., Brooks, P., Thompson, S., Feldman, C., Willingale, R., Button, T., Rodriguez Sanmartin, D., Zhang, D., James, A., Theobald, C., Willis, G. & Smith, A. (2009). *Proc. SPIE*, **7360**, 736008.
- Barbera, M., Candia, R., Collura, A., Di Cicca, G., Pellicciari, C., Sciortino, S. & Varisco, S. (2006). *Proc. SPIE*, **6266**, 62663F.
- Basso, S., Cotroneo, V. & Pareschi, G. (2008). *Mem. Soc. Astron. It.* **79**, 224.
- Civitani, M., Basso, S., Ghigo, M., Pareschi, G., Salmaso, B., Spiga, D., Tagliaferri, G., Vecchi, G., Burwitz, V., Hartner, G. D. & Menz, B. (2014). *Proc. SPIE*, **9144**, 914416.
- Civitani, M., Ghigo, M., Basso, S., Proserpio, L., Spiga, D., Salmaso, B., Pareschi, G., Tagliaferri, G., Burwitz, V., Hartner, G., Menz, B., Bavdaz, M. & Wille, E. (2013). *Proc. SPIE*, **8861**, 886110.
- Collon, M., Ackermann, M., Günther, R., Chatbi, A., Vacanti, G., Vervest, M., Yanson, A., Beijersbergen, M., Bavdaz, M., Wille, E., Haneveld, J., Olde Riekerink, M., Koelewijn, A., van Baren, C., Müller, P., Krumrey, M., Burwitz, V., Sironi, G. & Ghigo, M. (2014). *Proc. SPIE*, **9144**, 91442G.
- Collura, A., Barbera, M., Inzerillo, G., Mirabello, F., Sciortino, S. & Serio, S. (1994). *Proc. SPIE*, **2280**, 206–213.
- Craig, W. W., An, H. & Blaedel, K. L. (2011). *Proc. SPIE*, **8147**, 81470M.
- Dell'Agostino, S., Riva, M., Spiga, D., Basso, S. & Civitani, M. (2014). *Proc. SPIE*, **9150**, 915021.
- Fürmetz, M., Eder, J., Pfeffermann, E. & Predehl, P. (2014). *Proc. SPIE*, **9144**, 91444X.
- Ghigo, M., Proserpio, L., Basso, S., Citterio, O., Civitani, M., Pareschi, G., Salmaso, B., Sironi, G., Spiga, D., Tagliaferri, G., Vecchi, G., Zambra, A., Parodi, G., Martelli, F., Gallieni, D., Tintori, M., Bavdaz, M., Wille, E., Ferrario, I. & Burwitz, V. (2013). *Proc. SPIE*, **8884**, 88841Q.
- Pareschi, G., Basso, S., Bavdaz, M., Citterio, O., Civitani, M. M., Conconi, P., Gallieni, D., Ghigo, M., Martelli, F., Parodi, G., Proserpio, L., Sironi, G., Spiga, D., Tagliaferri, G., Tintori, M., Wille, E. & Zambra, A. (2011). *Proc. SPIE*, **8147**, 81470L.
- Proserpio, L., Breunig, E., Friedrich, P. & Winter, A. (2014). *Proc. SPIE*, **9144**, 91445L.
- Raimondi, L. & Spiga, D. (2015). *Astron. Astrophys.* **573**, A22.
- Reid, P. B., Aldcroft, T. L., Allured, R., Cotroneo, V., Johnson-Wilke, R. L., Marquez, V., McMuldroy, S., O'Dell, S. L., Ramsey, B. D., Schwartz, D. A., Troler-McKinstry, S. E., Vikhlinin, A. A., Wilke, R. H. T. & Zhao, R. (2014). *Proc. SPIE*, **9208**, 920807.
- Roddy, F. (1988). *Appl. Opt.* **27**, 1223.
- Salmaso, B., Basso, S., Brizzolari, C., Civitani, M., Ghigo, M., Pareschi, G., Spiga, D., Tagliaferri, G. & Vecchi, G. (2014). *Proc. SPIE*, **9151**, 91512W.
- Schwartz, D., Allured, R., Bookbinder, J., Cotroneo, V., Forman, W., Freeman, M., McMuldroy, S., Reid, P., Tananbaum, H., Vikhlinin, A., Johnson-Wilke, R. L., Troler-McKinstry, S. E., Wilke, R. H. T., Jackson, T. N., Ramirez, J. I., Gubarev, M. V., Kolodziejczak, J. J., O'Dell, S. L. & Ramsey, B. D. (2014). *Proc. SPIE*, **9208**, 920806.
- Spiga, D., Barbera, M., Basso, S., Civitani, M., Collura, A., Dell'Agostino, S., Lo Cicero, U., Lullo, G., Pellicciari, C., Riva, M., Salmaso, B. & Sciortino, L. (2014). *Proc. SPIE*, **9208**, 92080A.
- Spiga, D., Basso, S., Bavdaz, M., Burwitz, V., Civitani, M., Citterio, O., Ghigo, M., Hartner, G., Menz, B., Pareschi, G., Proserpio, L., Salmaso, B., Tagliaferri, G. & Wille, E. (2013a). *Proc. SPIE*, **8861**, 88611F.
- Spiga, D., Raimondi, L., Svetina, C. & Zangrando, M. (2013b). *Nucl. Instrum. Methods Phys. Res. A*, **710**, 125.
- Van Speybroeck, L. P. & Chase, R. C. (1972). *Appl. Opt.* **11**, 440.
- Winter, A., Breunig, E., Friedrich, P. & Proserpio, L. (2014). *Proc. SPIE*, **9144**, 91441C.